JOURNAL OF GUIDANCE, CONTROL, AND DYNAMICS
Vol. 35, No. 2, March–April 2012

Nonredundant Single-Gimbaled Control Moment Gyroscopes

Timothy A. Sands,* Jae Jun Kim,† and Brij N. Agrawal‡
Naval Postgraduate School, Monterey, California 93943

DOI: 10.2514/1.53538

Two objectives dominate consideration of control moment gyroscopes for spacecraft maneuvers: high torque (equivalently momentum) and singularity-free operations. This paper adds to the significant body of research toward these two goals using a minimal three-control-moment-gyroscope array to provide significant singularity-free momentum performance increase spherically (in all directions) by modification of control-moment-gyroscope skew angles, compared with the ubiquitous pyramid geometry skewed at 54.73 deg. Spherical 1*H* (one control moment gyroscope's worth momentum) singularity-free momentum is established with bidirectional 1*H* and 2*H* in the third direction in a baseline configuration. Next, momentum space reshaping is shown via mixed skew angles permitting orientation of maximum singularity-free angular momentum into the desired direction of maneuver (yaw in this study). Finally, a decoupled gimbal angle calculation technique is shown to avoid loss of attitude control associated with singular matrix inversion. This technique permits 3*H* (maximal) yaw maneuvers without loss of attitude control despite passing through singularity. These claims are demonstrated analytically, then heuristically, and finally validated experimentally.

Nomenclature

$[A]$	=	gradient matrix of gimbal angles and skew angle(s) with respect to gimbal rotation angle
c	=	cosine function
det	=	determinant
H	=	total momentum vector $\{h_x \quad h_y \quad h_z\}^T$
$\|H\|$	=	magnitude of total angular momentum of the array of control moment gyroscopes
Hs	=	total momentum magnitude of control-moment-gyroscope array when encountering a singular condition
$h_{x,y,z}$	=	momentum in the x, y, and z directions (normalized by one control moment gyroscope's worth of momentum)
s	=	sine function
β_i	=	skew angle for ith control moment gyroscope
$\partial h_x/\partial\theta_i$	=	Partial derivative of momentum in x-direction taken with respect to ith gimbal rotation angle
θ_i	=	gimbal rotation angle for ith control moment gyroscope
$\dot{\theta}_i$	=	gimbal rotation rate for ith control moment gyroscope
$1H$, $2H$, $3H$	=	normalized angular momentum output by one, two, and three control moment gyroscopes
$4H$	=	normalized angular momentum output by four control moment gyroscopes (also called saturation)

I. Introduction

RAPID spacecraft reorientation often drives design engineers to consider control moment gyroscopes (CMGs). CMGs are momentum exchange devices that exhibit extreme torque magnification (i.e., for a small amount of torque input to the CMG gimbal motors, a large resultant output torque is achieved) but inherently possess singular directions, where no torque can be generated. Despite singularity issues, CMG research began in the 1960s for large satellites like Skylab (which used three double-gimbaled CMGs, or DGCMGs) [1]. Computers of the time could not perform matrix inversion in real time. Simple systems that did not require matrix inversion were an obvious choice. Otherwise, algorithmically simple approximations must have been available for the system chosen. CMG steering and singularity avoidance was researched a lot in the 1970s, 1980s, and 1990s [2–11].

Singularity avoidance was typically done using a gradient method and DGCMGs [5,6,12]. These gradient methods are not effective for single-gimbaled CMGs (SGCMGs) like they are for DGCMGs. Magulies and Aubrun were the first to formulate a theory of singularity and control [7] including the geometric theory of singular surfaces, the generalized solution of the output equation, null motion (using greater than three SGCMGs), and the possibility of singularity avoidance for general SGCMG systems. Also, in 1978, Russian researcher Tokar published singularity surface shape description, size of work space, and considerations of gimbal limits [8].

Kurokawa et al. identified that a system such as a pyramid type SGCMG system will contain an impassable singular surface and concluded systems with no less than six units provide adequate work space free of impassable singular surfaces [17]. The Mir space station was designed for six-SGCMG operations. The research contained in this paper evaluates singularity-free operations using a mere three-CMG array by reducing singularities and then penetrating those remaining singularities without loss of attitude control.

Continued research aimed at improving results with less than six CMGs emphasized a four-CMG pyramid [14]. Much research resulted in gradient methods that regarded passability as a local problem that proved problematic [13,15,16]. Global optimization was also attempted but proved problematic in computer simulations [17–19]. Difficulties in global steering were also revealed in [20]. Reference [21] compared six different independently developed steering laws for pyramid-type SGCMG systems. The study concluded that exact inverse calculation was necessary (the exact inverse calculation is used in this paper). Other researchers addressed the inverted matrix itself, adding components that made the matrix robust to inversion singularity [22–24] as extensions of the approach to minimize the error in generalized inverse Jacobian calculation [25]. These approaches introduced tracking errors where necessary to avoid singularities by following a different momentum path (generating other-than-desired torque). Reference [26] sought to use a hybrid steering logic to maintain attitude tracking precision while avoiding hyperbolic internal singularities or escaping elliptic singularities with a four-CMG array skewed at 54.73 deg, the ubiquitous baseline described in [14] and depicted in Fig. 1.

Received 21 December 2010; accepted for publication 15 September 2011.

*Assistant Professor; tasands@nps.edu. Member AIAA.
†Research Assistant Professor; jki12@nps.navy.mil.
‡Distinguished Professor; agrawal@nps.edu.

Report Documentation Page

Form Approved
OMB No. 0704-0188

1. REPORT DATE	2. REPORT TYPE	3. DATES COVERED
APR 2012		**00-00-2012 to 00-00-2012**

4. TITLE AND SUBTITLE	5a. CONTRACT NUMBER
Nonredundant Single-Gimbaled Control Moment Gyroscopes	5b. GRANT NUMBER
	5c. PROGRAM ELEMENT NUMBER
6. AUTHOR(S)	5d. PROJECT NUMBER
	5e. TASK NUMBER
	5f. WORK UNIT NUMBER
7. PERFORMING ORGANIZATION NAME(S) AND ADDRESS(ES) **Naval Postgraduate School,Monterey,CA,93943**	8. PERFORMING ORGANIZATION REPORT NUMBER
9. SPONSORING/MONITORING AGENCY NAME(S) AND ADDRESS(ES)	10. SPONSOR/MONITOR'S ACRONYM(S)
	11. SPONSOR/MONITOR'S REPORT NUMBER(S)

12. DISTRIBUTION/AVAILABILITY STATEMENT
Approved for public release; distribution unlimited

13. SUPPLEMENTARY NOTES

14. ABSTRACT

15. SUBJECT TERMS

16. SECURITY CLASSIFICATION OF:			17. LIMITATION OF ABSTRACT	18. NUMBER OF PAGES	19a. NAME OF RESPONSIBLE PERSON
a. REPORT	b. ABSTRACT	c. THIS PAGE			
unclassified	**unclassified**	**unclassified**	**Same as Report (SAR)**	**10**	

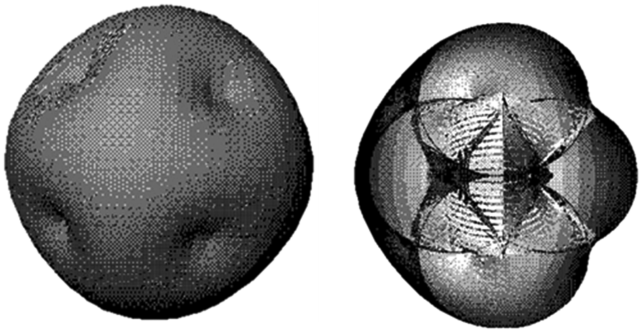

Fig. 1 Singularity surfaces associated with the ubiquitous skew angle of 54.73 deg.

Momentum path planning is another approach used to attempt to avoid singularities that can also achieve optimization if you have knowledge of the command sequence in the near future [25,27,28]. Another method used to avoid singularities is to use null motion to first reorient the CMGs to desired gimbal positions that are not near singular configurations [29]. By definition, null motion is motion of the CMGs that results in a net zero torque. Null motion only exists when more than three SGCMGs are used. The extra degrees of freedom provided by a redundant configuration with more than three SGCMGs are used to execute the null motion. Despite the massive amount of research done on CMGs, precision control with CMGs (especially only three SGCMGs, a nonredundant configuration) is still an unsolved problem [28,30,31]. This research paper investigates a modification of the four-CMG pyramid. Here, only three CMGs are used; thus, the problem is nonredundant: three-axis control is accomplished by exactly three degrees of freedom. There will not be an extra degree of freedom to use a constraint equation for singularity avoidance. Furthermore, this paper will describe methods to exactly follow the commanded path to minimize tracking errors rather than a path that avoids singularities.

Typical CMG output torques are on the order of hundreds to thousands of times the torque output of reaction wheels, another kind of momentum exchange attitude control actuator. A unique challenge of CMG implementation remains the mathematical singularity. Arguably, the most common configuration for a skewed array of four CMGs is the pyramid array where the four CMGs are skewed at an angle of $\beta = 54.73$ deg, resulting in an optimal spherical momentum capability [1] requiring internal singularity avoidance [1–8,32–37]. The desire is often stated as an equivalent (spherical), maximized momentum capability (not singularity-free) in all directions based on the $\{++++\}$ or $\{----\}$ $0H$ and $4H$ saturation singularities, where all four CMGs are pointing in the same direction (Fig. 2). The typical design approach may be succinctly stated: 1) optimize spherical momentum, and then 2) minimize impact of singularities. The approach adopted here will reverse the traditional approach as follows: 1) minimize singularities, and then 2) maximize spherical momentum. Surprisingly, the result turns out quite differently. This paper begins by comparing performance of a three of four (3/4)-skewed pyramid using the baseline skew angle $\beta = 54.73$ deg (derived from the four-CMG pyramid) to the performance of a 3/4 CMG pyramid with the skew angle specifically optimized for maximum singularity-free angular momentum. It will be shown that a 3/4 CMG pyramid skewed at $\beta = 54.73$ deg can achieve a maximum singularity-free momentum of 15% of one CMG's maximal momentum, while the proposed geometry can achieve 100% of one CMG's maximal momentum in all directions with superior performance in a preferred direction.

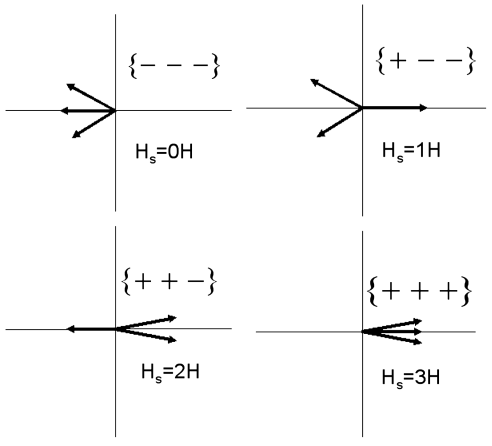

Fig. 2 Individual CMG momentum directions for a 3/4 CMG skewed array in a singular configuration of gimbal angles.

II. Torque Generation and Singularities

To achieve a specified output torque from a CMG array, a command must be sent to the gimbal motor. Equations (1–4) derive this relationship for $i = n$ CMGs normalized by one CMG's worth of momentum ($1H$). First, write the angular momentum vectors h_x, h_y, and h_z in x, y, and z directions composed of components of angular momentum contributions of the three CMGs combining to form the overall system angular momentum vector $\mathbf{H}$. It is desirable to express the rate of change of angular momentum $\dot{\mathbf{H}}$ in order to use the first-principles Newton–Euler relationship between the rate of change of angular momentum and the applied external torques. The rate of change of angular momentum $\dot{\mathbf{H}}$ may be decomposed into the gradient with respect to the gimbal angles $\partial\mathbf{H}/\partial\boldsymbol{\theta}_i$ multiplied by the rate of change of the gimbal angles $\{\dot{\boldsymbol{\theta}}\}$. CMGs are inclined so gimbal planes form skew angles β_i with respect to the xy plane as depicted in Fig. 2, where $i = 1 - 3$ for three CMGs.. Begin by writing equations for each momentum vector in xyz coordinates for three CMGs normalized by $1H$:

$$\left.\begin{aligned} \mathbf{h_x} &= \mathbf{\cos\theta_3 - \cos\theta_1 + \cos\beta_2 \sin\theta_2} \\ \mathbf{h_y} &= \mathbf{\cos\beta_3 \sin\theta_3 - \cos\beta_1 \sin\theta_1 - \cos\theta_2} \\ \mathbf{h_z} &= \mathbf{\sin\beta_1 \sin\theta_1 + \sin\beta_2 \sin\theta_2 + \sin\beta_3 \sin\theta_3} \end{aligned}\right\} \tag{1a}$$

$$\left.\begin{aligned} \mathbf{h_x} &= \cos\theta_3 - \cos\theta_1 + \cos\beta \sin\theta_2 \quad \mathbf{h_y} = \cos\beta(\sin\theta_3 - \sin\theta_1) \\ &- \cos\theta_2 \mathbf{h_z} = \mathbf{\sin\beta(\sin\theta_1 + \sin\theta_2 + \sin\theta_3)} \end{aligned}\right\} \tag{1b}$$

$$\mathbf{H} = \mathbf{h_x}\hat{x} + \mathbf{h_y}\hat{y} + \mathbf{h_z}\hat{z} \tag{2a}$$

$$\frac{\partial \mathbf{H}}{\partial \boldsymbol{\theta}_i} = \begin{Bmatrix} \frac{\partial \mathbf{h_x}}{\partial \boldsymbol{\theta}_i} \\ \frac{\partial \mathbf{h_y}}{\partial \boldsymbol{\theta}_i} \\ \frac{\partial \mathbf{h_z}}{\partial \boldsymbol{\theta}_i} \end{Bmatrix} = \underbrace{\begin{bmatrix} \sin\theta_1 & \cos\beta\cos\theta_2 & -\sin\theta_3 \\ -\cos\beta\cos\theta_1 & \sin\theta_2 & \cos\beta\cos\theta_3 \\ \sin\beta\cos\theta_1 & \sin\beta\cos\theta_2 & \sin\beta\cos\theta_3 \end{bmatrix}}_{[A]}$$

$$= [A] \tag{2b}$$

The [**A**] matrix (containing gimbal angles θ_i and skew angles β_i) must be inverted to find the required CMG gimbal command for commanded output torque per Eq. (3). The Newton–Euler relation relates generated torque to the timed rate of change of angular momentum of the spacecraft system. A CMG absorbs momentum change $\dot{\mathbf{H}}$, causing an equal and opposite change in momentum on the spacecraft. For n CMGs, the general relation is

$$\dot{\mathbf{H}} = \frac{\partial \mathbf{H}}{\partial \boldsymbol{\theta}} \frac{\partial \boldsymbol{\theta}}{\partial t} = \frac{\partial \mathbf{H}}{\partial \boldsymbol{\theta}} \dot{\boldsymbol{\theta}} = \sum_{\mathbf{i}=\mathbf{1}}^{\mathbf{n}} \mathbf{h_i} = \sum_{\mathbf{i}=\mathbf{1}}^{\mathbf{n}} \mathbf{a_i}(\theta_i)\dot{\boldsymbol{\theta}}_\mathbf{1} = [A]\{\dot{\boldsymbol{\theta}}\}$$
$$\rightarrow [A]^{-1}\{\dot{\mathbf{H}}\} = [A]^{-1}[A]\{\dot{\boldsymbol{\theta}}\} = \{\dot{\boldsymbol{\theta}}\} \tag{3}$$

For some combinations of gimbal and skew angles, the [**A**] matrix columns can become linearly dependent. At these combinations of skew and gimbal angles, the determinant of the [**A**] matrix becomes zero, leading to singular inversion as follows:

$$\det[A] = s\beta\{s\theta_2[s(\theta_1 + \theta_2)] + c\beta c\theta_2[s(\theta_3 - \theta_1) + 2c\theta_1 c\theta_3 c\beta]\} \tag{4}$$

where s = sine, and c = cosine.

III. Three of Four Skewed Control Moment Gyroscope Array

The 3/4 CMG array modifies the commonly studied four-CMG skewed pyramid. A minimum of three CMGs is required for three-axis control, and the fourth is often used for singularity avoidance. With the 3/4 array, only three CMGs are used for active attitude control with the fourth CMG held in reserve for robust failure properties. The fourth CMG is not active (dormant), with no electrical power applied to its gimbal motor until required by the loss of a failing CMG. When a CMG fails, it may be despun (controlled) and then depowered while the spare CMG is powered and spun up (again controlled). Thus, the fourth CMG substitutes the failing CMG, maintaining a 3/4 CMG array configuration. The 3/4 CMG array remains the focus of this research, and the results here can be equally applied to the new (substituted) 3/4 CMG array. Experimental verification will be provided in later sections using a spacecraft testbed with a 3/4 CMG array containing a balance mass in the place of the fourth CMG (Fig. 2).

The approach taken by the authors is to first optimize the 3/4 skewed array (system of four CMGs in a skewed configuration where only three CMGs operate for attitude control) geometry itself by choosing the skew angle that provides the greatest singularity-free momentum. At this optimal singularity-free skew angle, the 3/4 CMG array can operate at momentum values less than the singularity-free threshold without any kind of singularity avoidance scheme. Furthermore, utilization of mixed skew angles can rotate the work space to maximize momentum in a preferred direction, again singularity-free. Yaw is the preferred direction in this study. A direct comparison with the traditional optimal spherical skew angle will demonstrate the dramatic improvement in torque capability of the CMG array. Analytical derivation is followed by heuristic, geometric analysis, and then validation via experimentation on a realistic spacecraft simulator in ground tests.

IV. Analysis

Singular combinations of gimbal angles and skew angles can be determined analytically by examining the determinant of the [**A**] matrix. Recall

$$\det[A] = s\beta\{s\theta_2[s(\theta_1 + \theta_2)] + c\beta c\theta_2[s(\theta_3 - \theta_1) + 2c\theta_1 c\theta_3 c\beta]\}$$

When the determinant goes to zero, the matrix has linearly dependent columns resulting in singular inversion. There are six cases (with multiple subcases) that result in a singular [**A**] matrix (less than full rank) with $\beta_i = \beta$, where each singular case is caused by a component quantity being equal to zero resulting in the total quantity not being invertible (see Table 1):

Table 1 Six singular cases where $\det[A] = 0$

Case	Value
1	$\sin\beta = 0$
2	$\sin(\theta_1 + \theta_3) = \sin(\theta_3 - \theta_1) = 0$
3	$\sin\theta_2[\sin(\theta_1 + \theta_3)] + \cos\beta\cos\theta_2[\sin(\theta_3 - \theta_1) + 2\cos\theta_1\cos\theta_3\cos\beta] = 0$
4	$\sin\theta_2 = 0$
5	$\sin(\theta_1 + \theta_3) = \cos\theta_2 = 0$
6	$\sin(\theta_1 + \theta_3) = \cos\theta_2 = 0$

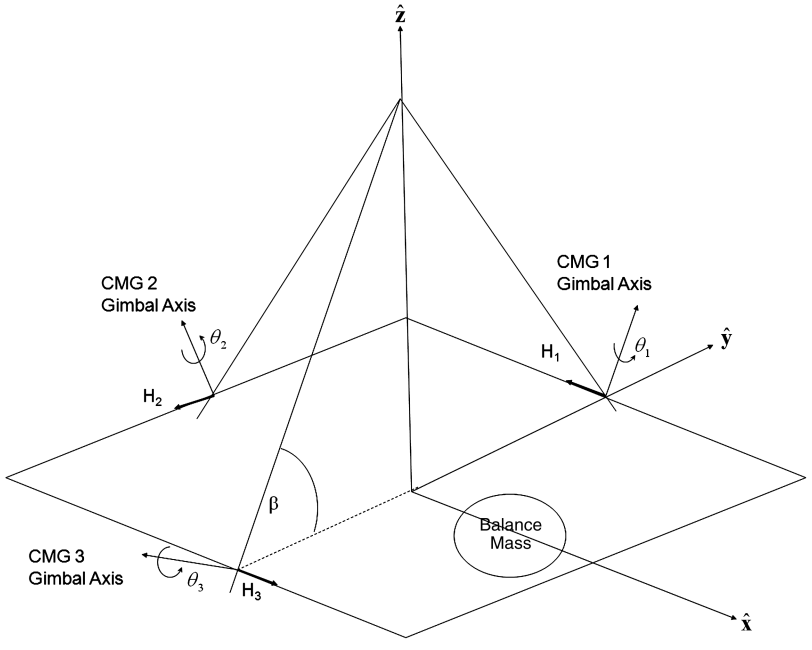

Fig. 3 3/4 skewed CMG array used in this study.

Case 1:

$$\underbrace{\sin\beta}_{0}\{\sin\theta_2[\sin(\theta_1+\theta_3)]+\cos\beta\cos\theta_2[\sin(\theta_3-\theta_1)+2\cos\theta_1\cos\theta_3\cos\beta]\}\rightarrow\sin\beta=0 \tag{5}$$

Case 2:

$$\sin\beta\{\sin\theta_2\underbrace{[\sin(\theta_1+\theta_3)]}_{0}+\cos\beta\cos\theta_2\underbrace{[\sin(\theta_3-\theta_1)}_{0}+2\cos\theta_1\cos\theta_3\cos\beta]\}\rightarrow\sin(\theta_1+\theta_3)=0\quad\text{and}\quad\sin(\theta_3-\theta_1)=0 \tag{6}$$

Case 3:

$$\sin\beta\underbrace{\{\sin\theta_2[\sin(\theta_1+\theta_3)]+\cos\beta\cos\theta_2[\sin(\theta_3-\theta_1)+2\cos\theta_1\cos\theta_3\cos\beta]\}}_{0}\rightarrow\sin\theta_2[\sin(\theta_1+\theta_3)]+\cos\beta\cos\theta_2[\sin(\theta_3-\theta_1)+2\cos\theta_1\cos\theta_3\cos\beta]=0 \tag{7}$$

Case 4:

$$\sin\beta\{\underbrace{\sin\theta_2}_{0}[\sin(\theta_1+\theta_3)]+\underbrace{\cos\beta\cos\theta_2}_{0}[\sin(\theta_3-\theta_1)+2\cos\theta_1\cos\theta_3\cos\beta]\}\rightarrow\sin\theta_2=0\quad\text{and}\quad\cos\beta\cos\theta_2=0 \tag{8}$$

Case 5:

$$\sin\beta\{\sin\theta_2\underbrace{[\sin(\theta_1+\theta_3)]}_{0}+\underbrace{\cos\beta\cos\theta_2}_{0}[\sin(\theta_3-\theta_1)+2\cos\theta_1\cos\theta_3\cos\beta]\}\rightarrow\sin(\theta_1+\theta_3)=0\quad\text{and}\quad\cos\beta\cos\theta_2=0 \tag{9}$$

Case 6:

$$\sin\beta\{\underbrace{\sin\theta_2}_{0}[\sin(\theta_1+\theta_3)]+\cos\beta\cos\theta_2\underbrace{[\sin(\theta_3-\theta_1)+2\cos\theta_1\cos\theta_3\cos\beta]}_{0}\}\rightarrow\sin\theta_2=0\quad\text{and}\quad\sin(\theta_3-\theta_1)+2\cos\theta_1\cos\theta_3\cos\beta=0 \tag{10}$$

There are a few trivial cases. Nontrivial cases may be analyzed as follows. In general, for a given skew angle, each case produces gimbal angle combinations that result in $\det[\mathbf{A}]=0$. These gimbal combinations may be used to calculate the resultant momentum at the singular condition. Minimum singular momentum values may then be plotted for iterated skew angles 0 deg $<\beta<$ 90 deg. Having established the minimum value of momentum at singular combinations of gimbal angles, it is not possible to become singular at momentum less than these values (Fig. 3). Thus, the result is the maximum singularity-free momentum space. As we see in Fig. 3, the extensively studied skew angle ($\beta = 54.73$ deg), which is originally optimized for maximal momentum performance of four CMGs (not singularity-free momentum), yields roughly $0.15H$ momentum before reaching a singular state for three CMGs. To avoid singularities and maintain attitude control, spacecraft control torque is limited to less than $0.15H$. Thus, using the ubiquitous skew angle of 54.73 deg, which was optimized for spherical maximum momentum (not singularity free) with four SGCMGs, in the case of three CMGs only, 15% of one CMG's torque is achievable singularity free. Using the new skew angle of $\beta = 90$ deg (see Figs. 4 and 5), which was optimized for singularity-free momentum space, $1.0H$ (100% the momentum capability of one CMG) is achievable singularity-free in any direction. Theoretically, singularity-free momentum is increased from roughly $0.15H$ to $1H$: $(1H-0.15H)/0.15H > 500\%$. This theoretical claim must be validated. To do so, Sec. V will provide simulated visual depictions of the singularity surfaces in the momentum space demonstrating a lack of singularities in the momentum space less than $1H$, and then Sec. VII will provide experiments that command maneuvers resulting in angular momentum trajectories that exceed $0.15H$ while monitoring the condition of the $[A]$ matrix for potential singularities. If the inverse condition number of the $[A]$ matrix ever goes to zero, the CMGs have encountered a singularity. It will be shown that the CMGs remain singularity free as claimed (see Fig. 4).

V. Heuristics

The preceding analysis reveals singularity-free operations less than $1H$ in all directions by implication. While useful, the analysis certainly does not yield much intuition for the attitude control engineer to design safe momentum trajectories through the momentum space. Are there directions that can exceed $1H$ singularity-free?

Advances in computer processor speeds make a heuristic approach readily available. Consider rotating a vector 360 deg creating a CMG gimbal cutting plane (discretized at some interval). Then, rotate the gimbal plane 360 deg, creating a lattice of discrete points forming a solid, filled sphere. This lattice provides discretized points to analyze CMG array momentum. This may be done in embedded loops of computer code. Each discrete point corresponds to a set of three

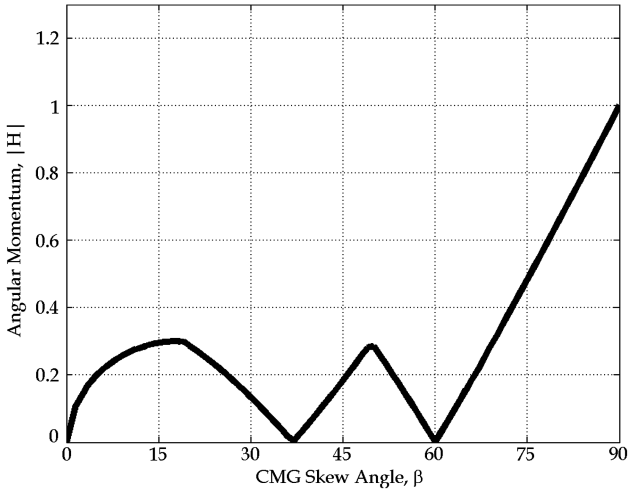

Fig. 4 Skew angle optimization for maximum singularity-free normalized momentum.

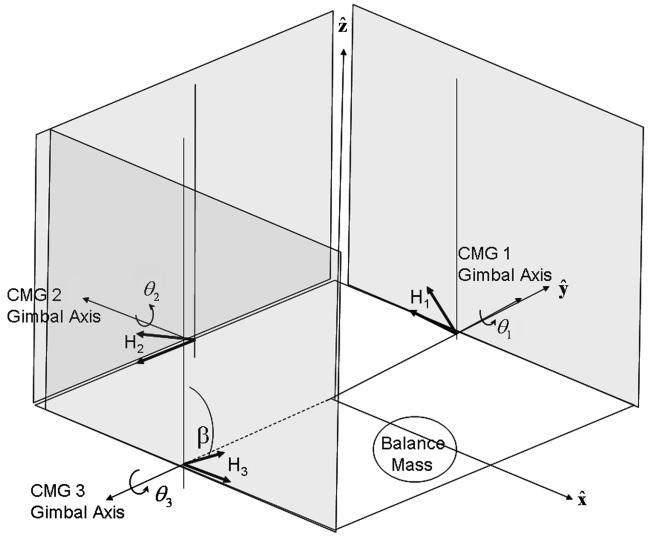

Fig. 5 3/4 CMG skewed array momentum cutting planes with $\beta = 90$ deg.

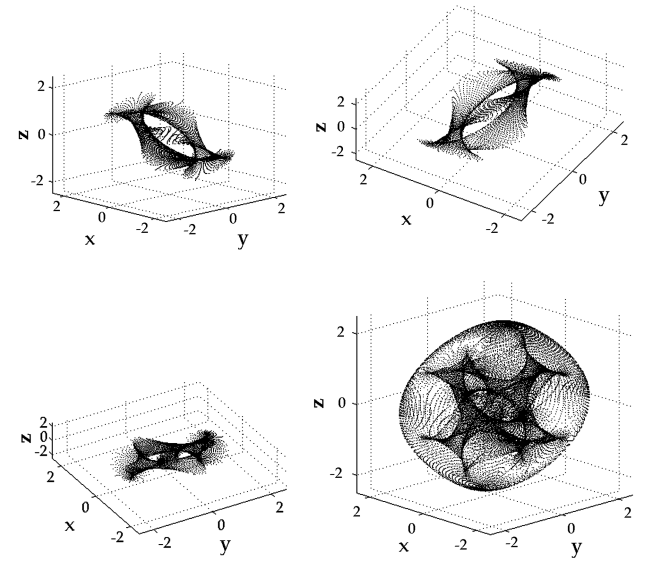

Fig. 6 Singular surfaces for a traditional 3/4 CMG skewed array at a skew angle of 54.73 deg..

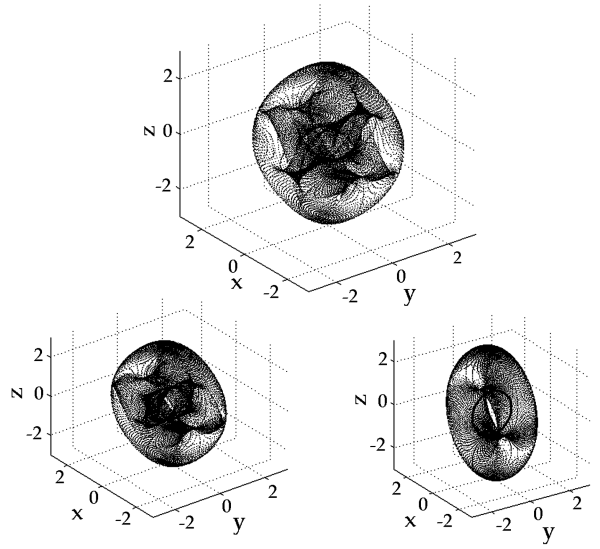

Fig. 7 Skew iteration at 70 deg (top), 80 deg (lower left), and 90 deg (lower right).

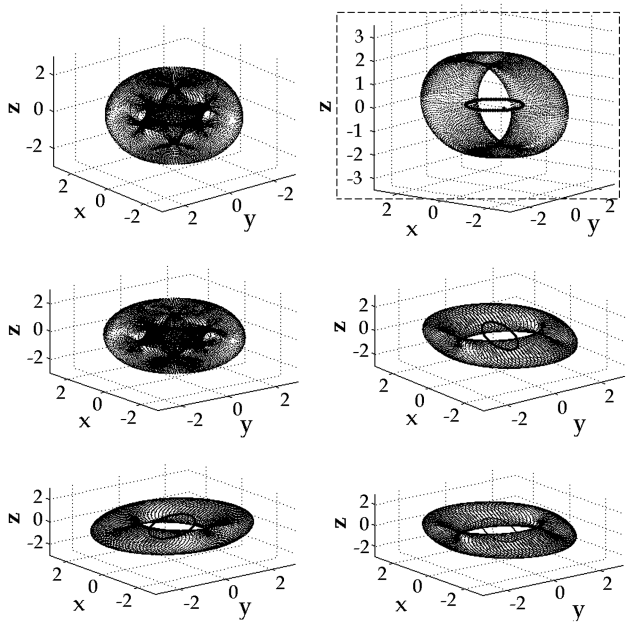

Fig. 8 Mixed skew angles (see Table 2) highlighting case 2 $\{90, 0, 90 \text{ deg}\}^T$.

coordinates or, equivalently, three gimbal angles. At each discrete point, the singularity/nonsingularity of [**A**] is established. At singular points, the normalized magnitude of angular momentum may be calculated. A point may be plotted at the magnitude of the momentum in the singular direction. This results in a three-dimensional singularity map granting intuition for maneuvering in the momentum space (e.g., Figs. 6–8). When the singular condition exists, one, two, or three CMGs' angular momentums may be generating momentum in the same direction, and this fact leads to the nomenclature listed in Fig. 5, which is ubiquitously used in the literature (e.g., [37]). If all three CMGs point in the same positive or negative direction ($0H$ and $3H$), this represents the maximum capability of the array, and the singularity is referred to as saturation. Other singular cases that occur when one CMG is pointing opposed to the other two CMGs ($1H$) are referred to as internal.

Singular surfaces plotted in the momentum space (e.g., Figs. 6–8) result from several kinds of singularities: $0H$, $1H$, $2H$, and $3H$, depicted in Fig. 5. Typically, the optimal spherical skew angle is determined by the outer, saturation singular surface alone ($0H$ and $3H$ in the case of a $3/4$ CMG array). To find the maximum singularity-free skew angle, the analysis must also account for the $1H$ and $2H$ internal singularities.

It may be noted here that the often used optimal spherical skew angle ($\beta = 54.73$ deg) that results in equivalent momentum in all directions is derived using the $0H$ $\{- - - -\}$ and $4H$ $\{+ + + +\}$ singular surfaces of a four-CMG skewed array. The $0H$ and $4H$ singular surfaces are the saturation surfaces that result from all four CMGs pointing in the same direction, and their corresponding saturation surfaces for the $3/4$ array are the $0H$ and $3H$ singular surfaces. In the case of a $3/4$ CMG array, the singular surfaces are depicted in Fig. 6 for the often used optimal spherical momentum skew angle ($\beta = 54.73$ deg).

Note that the spherical nature of the external, saturation singular surfaces $\{+ + +\}$ and $\{- - -\}$ typified by the ubiquitous four-CMG pyramid array skewed at $\beta = 54.73$ deg (Fig. 1) are nearly maintained in the $3/4$ array. The internal $1H$ and $2H$ singularities are quite a problem, since they occupy a large portion of the momentum space. The combined singularity hypersurface makes it difficult to see a clear momentum path around the origin.

The typical design methodology might use the shape of the $3H$ outer momentum surfaces $\{+ + +\}$ and $\{- - -\}$ to define $\beta =$ 54.73 deg as the optimal spherical momentum skew angle. The attitude control engineer would be left with the task of maneuvering in this crowded momentum space while trying to avoid any point on

the singular hypersurface. Striking a singular point results in (at least temporary) loss of attitude control. Also note the maximum momentum capability is less than $3H$. Per Fig. 3, the maximum singularity-free momentum capability using $\beta = 54.73$ deg is $0.154868H$. If the skew angle were increased to 90 deg, Fig. 3 skew angle optimization indicates that, theoretically, singularity-free momentum would be increased $1.0H$. Consider the singular hypersurfaces for heuristic, geometric observations.

It was established in Sec. IV that a skew angle of 90 deg theoretically results in a singularity-free momentum space of $1H$ for the 3/4 CMG array. Repeating the numerical, heuristic singularity analysis as the skew angle increases is very revealing. Figure 7 displays the singular momentum space for a skew angle of 70, then 80, then 90 deg. Similar plots incremented every $\beta = 5$ deg are contained in [38], while these three examples in Fig. 7 are sufficient to demonstrate the behavior of increasing the skew angle. Notice how the $1H$ and $2H$ singular surfaces move away from the origin and gradually converge into each other as the skew angle increases to 90 deg. Fewer singular surfaces are obviously beneficial, but the vacancy of the center of the momentum space is especially significant, since it creates a significant portion of the momentum space that is free of singular conditions (free for maneuver without regard to singularities). Furthermore, it will be shown in the next section that the large area of singularity-free momentum space can be rotated via mixed skew angles to emphasize a preferred axis of rotation. The yaw axis is the preferred axis of maneuver in this study, but notice in Fig. 7 that greater angular momentum ($2H$) capability exists in the roll direction for this geometry of CMG array, while pitch maneuvers can achieve $1H$ singularity free. It is desirable to rotate the direction of maximum singularity-free momentum space to the yaw direction. It will be seen that mixed skew angles can rotate the momentum space to emphasize roll or pitch.

VI. Momentum Space Rotation: Mixed Skew Angles

Typically, skewed CMG arrays use identical skew angles for each CMG ($\beta_i = \beta$). By using mixed skew angles, the singularity-free football-shaped space can be reoriented to place the $2H$ momentum capability in the yaw direction. Six possible momentum reorientations are possible by laying down momentum planes from 90 to 0 deg, as listed in Table 2, resulting in rotations of the momentum space depicted, respectively, in Fig. 8. This section refers to fixed geometries and does not investigate the adaptive skew angle [39], especially since the adaptive skew angle provides an extra degree of freedom, while this research seeks to investigate what can be done with nonredundant configurations.

Notice (in Fig. 8) that three options for mixed skew angles result in the original momentum space rotated about $\hat{\mathbf{z}}$ such that $\hat{\mathbf{x}} \leftrightarrow \hat{\mathbf{y}}$, while two other options generate spherical momentum space filled with significant internal singularities. Notice the center of the momentum space is clogged with singular surfaces such that those two figures are blackened in the center. Our difficulty seeing the center is indicative of difficulties steering a momentum vector through that space without striking a singular surface for those two mixed skew angle combinations. This is an undesirable feature similar to the original case of four CMGs skewed at 54.73 deg (Fig. 1) or three CMGs skewed at 54.73 deg (Fig. 6) where only $0.15H$ was available singularity-free. This study seeks geometries with large areas of the momentum space that are free of singularities.

Table 2 Six possible combinations of mixed skew angles laying one or two momentum cutting planes from 0 to 90 deg[a]

β_1, deg	β_2, deg	β_3, deg
0	90	90
90[b]	0[b]	90[b]
90	90	0
0	0	90
0	90	0
90	0	0

[a]Corresponding singular hypersurfaces are depicted in Fig. 8, starting from the upper left and going to the lower right

[b]Special attention is brought to the case of $\{\beta_1, \beta_2, \beta_3\}^T = \{90, 0, 90 \text{ deg}\}^T$.

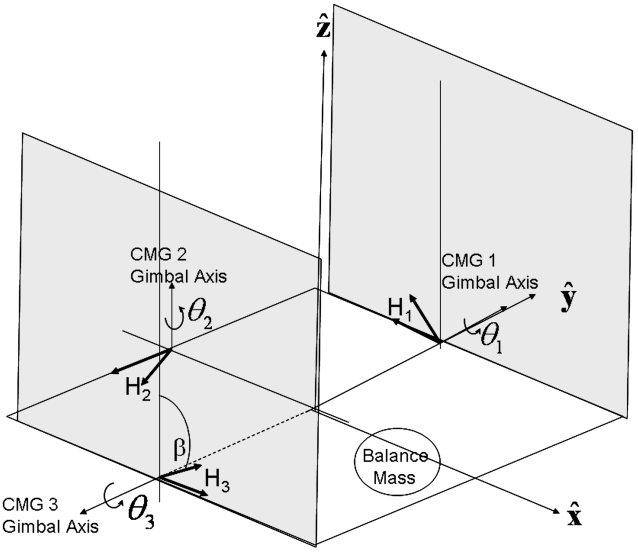

Fig. 9 $\{\beta_1, \beta_2, \beta_3\} = \{90, 0, 90 \text{ deg}\}$ mixed skew angle momentum cutting planes depicted for a 3/4 CMG skewed array.

One successful reorientation $\{\beta_1, \beta_2, \beta_3\} = \{90, 0, 90 \text{ deg}\}$ is accomplished by simply sliding the second CMG from 90 to 0 deg, resulting in singularity-free yaw momentum increase with a favorably vacant internal singularity structure. Figure 9 depicts a 3/4 CMG array skewed at mixed skew angles $\beta_1 = 90$ deg, $\beta_2 = 0$ deg, and $\beta_3 = 90$ deg. Trajectories originating at the origin of the momentum space have $1H$ spherical momentum capability and $2H$ momentum capability about yaw ($\hat{\mathbf{z}}$) singularity-free. Theoretically, singularity-free momentum is increased to $2H$ from $0.15H$ compared with the case of three CMGs skewed at 54.73 deg (Figs. 3 and 7): $(2H - 0.15H)/0.15H > 1000\%$. This claim must be experimentally validated. Section VIII provides experiments that command maneuvers resulting in angular momentum trajectories that exceed $0.15H$ and even exceed $1H$ (the demonstrated limit of singularity-free momentum space with nonmixed skew angles). Note that momentum trajectories that are initiated from points near (0,0,2) can traverse to $(0, 0, -2)$, resulting in $-4H$ being stored in the CMG array producing $+4H$ momentum imparted to the spacecraft about yaw singularity free.

VII. Experimental Verification: Skew Angle Optimization

Experimental verification of the singularity-free skew angle is performed on a free-floating three-axis spacecraft simulator to demonstrate singularity-free operations. The free-floating spacecraft testbed is referred to as TASS2 (three-axis spacecraft simulator) indicating its heritage as the second such testbed developed at the Naval Postgraduate School. The first testbed, TASS1 [40], was much smaller and did not use CMGs. A description of the experimental hardware is based on [38], for which the graphics were directly replicated here (Fig. 10). Figure 10 shows the actual picture of the three-axis simulator named as TASS2. The spacecraft bus simulator is supported on a spherical air bearing to simulate a weightless environment. A thin film of compressed air is injected between a spherical ball and a mating spherical cup. This thin film of air creates an essentially frictionless lubrication layer between the ball and cup. When test articles mounted to the ball segment are balanced, such that their aggregate center of gravity corresponds with the center of rotation of the ball, rotational motions of the ball and test articles match those of an object with similar inertial properties free falling

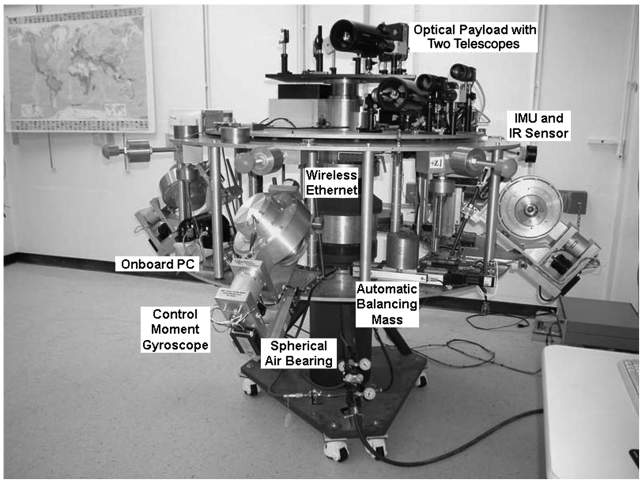

Fig. 10 TASS2, where IMU refers to inertial measurement unit.

though space. Because it is important to minimize the disturbance torque from any imbalance, three servolinear stages with lumped masses may be employed for automatic mass balancing. The three linear stages are placed parallel to the three spacecraft body axes but are not used in this study.

The spacecraft testbed payload is an optical relay for laser beams. The lower deck of the spacecraft is a bench model spacecraft with CMGs, active mass balancing system, fiber optic gyroscopes for attitude rate sensing, and typical onboard computers. The upper deck of the testbed is an experimental laser optical relay designed to accept a laser from the ground, aircraft, or space-based source and relay the laser to an uncooperative target on the ground, in the air, or in space. Description of the mission and some details about experimental hardware may be found in [40,41]. This laser relay mission demands rapid target acquisition yaw maneuvers in minimum time followed by fine pointing during target tracking.

To first demonstrate singularity-free operations (verify the large maneuver space is free of singular conditions as theoretically predicted earlier in this paper), experimental maneuvers were performed with a $+5$ deg yaw maneuver in 4 s followed by a -5 deg yaw maneuver in 4 s. The attitude is then regulated to zero while the CMG continues to output torque to counter gravity gradient disturbances typical of imbalanced ground test spacecraft simulators. The testbed has an autobalancing device to eliminate this gravity disturbance torque, but the device was disengaged to permit the experiment to explore more of the momentum space and to simplify assertions of CMG performance, since CMGs will be the only torque actuators. During previous research, this maneuver ($+5$ deg yaw maneuver in 4 s is followed by a -5 deg yaw maneuver in 4 s) was performed using a CMG geometry with skew angle of 57 deg (not depicted). The CMG array became singular, and the testbed spacecraft attitude control was lost, motivating this current study. The skew angle was increased to 90 deg for all three CMGs, and the

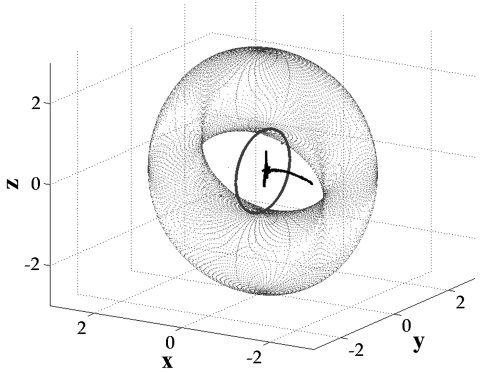

Fig. 11 Experiment: $+5$ deg yaw in 4 s, -5 deg yaw in 4 s, and then regulate for 5 min.

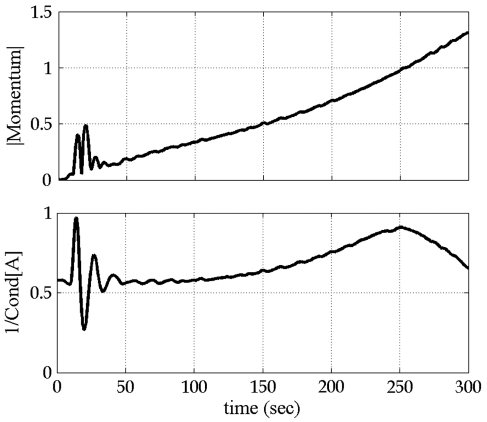

Fig. 12 Experiment: $+5$ deg yaw in 4 s, -5 deg yaw in 4 s, and then regulate for 5 min. Skew angles equal 90 deg.

identical experiment was repeated. Notice in Figs. 11 and 12 that the maneuver is performed and the testbed is regulated for 5 min. without striking any singular surfaces. Momentum magnitude and the inverse of the condition of the $[A]$ matrix verify this assertion.

Notice what happens when the same momentum trajectory is placed in the context of the theoretical singular momentum space of the optimal spherical skew angle $\beta = 54.73$ deg (Fig. 13). The internal singular surfaces are depicted individually for ease of visualization. This momentum trajectory is constantly close to the internal singular surfaces and quickly strikes a singular surface. A corresponding singular surface exists for a skew angle of 57 deg. Prior experiments using $\beta = 57$ deg went singular and resulted in the loss of attitude control when the momentum trajectory struck this corresponding singular surface.

VIII. Experimental Verification: Momentum Space Rotation

Next, experiments were performed with mixed skew angles to orient the maximum singularity-free momentum capability about the yaw axis, as seen in Figs. 14 and 15. The first experiment (Fig. 11) verified that momentum trajectories could exceed $1H$ in roll, but care was taken not to exceed $1H$ in yaw, since $1H$ defines the yaw limit for singularity-free operations of the {90, 90, 90 deg} configuration. To verify momentum space rotation here, we seek to verify that we can exceed $1H$ about yaw, so the yaw maneuvers were increased 160% in the same duration from 5 to 13 deg in only 4 s. This demands

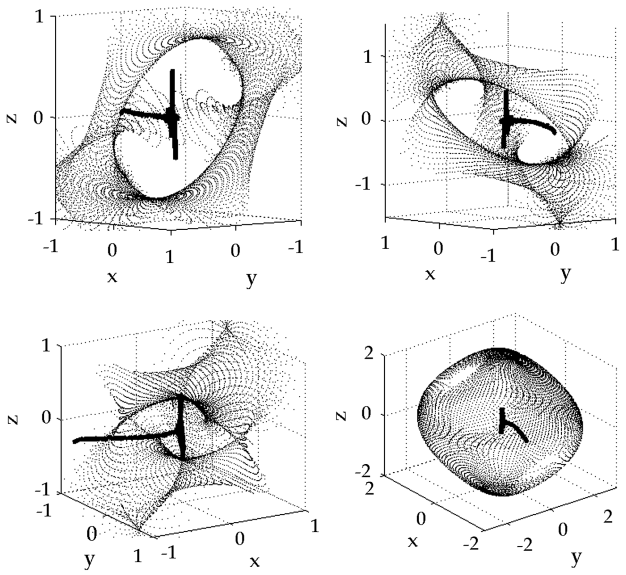

Fig. 13 Fictional experiment: Fig. 11 placed in context of 54.73 deg momentum envelope.

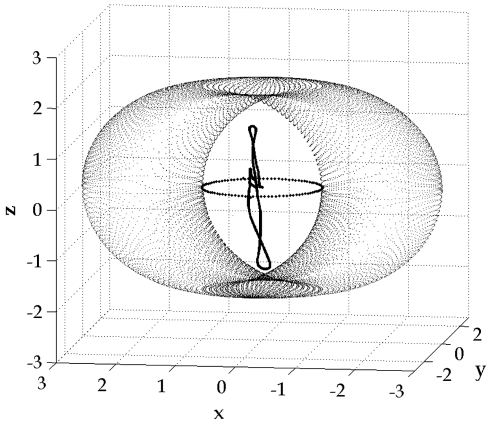

Fig. 14 Experimental results: +13 deg yaw in 4 s, and −13 deg yaw in 4 s performed in $\{\beta_1, \beta_2, \beta_3\} = \{90, 0, 90 \text{ deg}\}$ mixed skew angle configuration. the momentum trajectory is placed in the context of theoretical singular hypersurface.

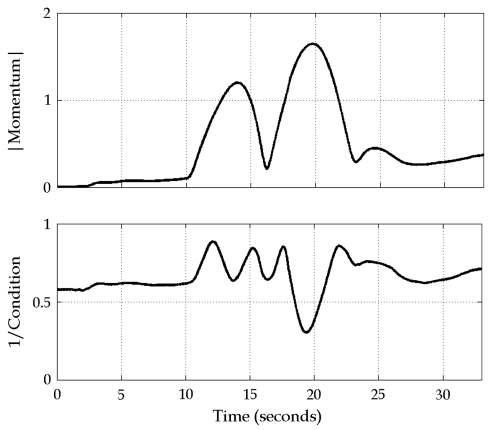

Fig. 15 Experimental results: +13 deg yaw in 4 s, and −13 deg yaw in 4 s performed in $\{\beta_1, \beta_2, \beta_3\} = \{90, 0, 90 \text{ deg}\}$ mixed skew angle configuration (with maneuver momentum and inverse condition of $[A]$).

significantly more momentum change, specifically about yaw. Per Figs. 14 and 15, the momentum is achieved singularity-free and the maneuver is performed without incident; thus, we see that the momentum space can be rotated to increase yaw maneuver capability.

IX. Analysis of Singularity Reduction: Decoupled Steering Commands Technique

In this section, we derive a strategy dubbed "decoupled control steering", where we take advantage of the simplifications that arise from the optimum singularity-free skew angle $\beta = 90$ deg, seeking to yield maximal ($3H$) momentum capability about yaw without loss of full attitude control. Substituting the $[A]$ matrix with $\beta = 90$ deg into Eq. (2) yields

$$\begin{Bmatrix} \dot{\theta}_1 \\ \dot{\theta}_2 \\ \dot{\theta}_3 \end{Bmatrix} = \underbrace{\begin{bmatrix} \sin\theta_1 & 0 & -\sin\theta_3 \\ 0 & \sin\theta_2 & 0 \\ \cos\theta_1 & \cos\theta_2 & \cos\theta_3 \end{bmatrix}^{-1}}_{\Downarrow} \begin{Bmatrix} \dot{h}_x \\ \dot{h}_Y \\ \dot{h}_Z \end{Bmatrix} \tag{11}$$

$$\begin{Bmatrix} \dot{\theta}_1 \\ \dot{\theta}_2 \\ \dot{\theta}_3 \end{Bmatrix} = \underbrace{\begin{bmatrix} \frac{c\theta_3}{c\theta_1 s\theta_3 + s\theta_1 c\theta_3} & \frac{-s\theta_3}{(c\theta_1 s\theta_3 + s\theta_1 c\theta_3)\tan\theta_2} & \frac{s\theta_3}{c\theta_1 s\theta_3 + s\theta_1 c\theta_3} \\ 0 & \frac{1}{s\theta_2} & 0 \\ \frac{-c\theta_1}{c\theta_1 s\theta_3 + s\theta_1 c\theta_3} & \frac{-s\theta_1}{(c\theta_1 s\theta_3 + s\theta_1 c\theta_3)\tan\theta_2} & \frac{s\theta_1}{c\theta_1 s\theta_3 + s\theta_1 c\theta_3} \end{bmatrix}}_{} \begin{Bmatrix} \dot{h}_x \\ \dot{h}_Y \\ \dot{h}_Z \end{Bmatrix} \tag{12}$$

Note that the y-momentum change equation has become decoupled from the x and z equations. Pitch momentum is determined completely by gimbal 2. The pitch equation may be separated from the matrix system of equations. The benefit is the elimination of singular gimbal commands for CMGs that are not in geometrically singular gimbal angle positions. Consider what happens if the first and third CMGs enter a combination of gimbal angles that satisfy $\cos\theta_1 \sin\theta_3 + \sin\theta_1 \cos\theta_3 = 0$. This would not result in singular commands to CMG gimbal 2. CMG gimbal 2 would receive the following command: $\dot{\theta}_2 = (1/\sin\theta_2)\dot{h}_y$. The individual equations for each of the three CMGs to be implemented are

$$\begin{aligned}
\dot{\theta}_1 &= \frac{\cos\theta_3}{\cos\theta_1 \sin\theta_3 + \sin\theta_1 \cos\theta_3}\dot{h}_x \\
&\quad + \frac{-\sin\theta_3}{(\cos\theta_1 \sin\theta_3 + \sin\theta_1 \cos\theta_3)\tan\theta_2}\dot{h}_y \\
&\quad + \frac{\sin\theta_3}{\cos\theta_1 \sin\theta_3 + \sin\theta_1 \cos\theta_3}\dot{h}_z \\
\dot{\theta}_2 &= \frac{1}{\sin\theta_2}\dot{h}_Y \\
\dot{\theta}_3 &= \frac{-\cos\theta_1}{\cos\theta_1 \sin\theta_3 + \sin\theta_1 \cos\theta_3}\dot{h}_x \\
&\quad + \frac{-\sin\theta_1}{(\cos\theta_1 \sin\theta_3 + \sin\theta_1 \cos\theta_3)\tan\theta_2}\dot{h}_y \\
&\quad + \frac{\sin\theta_1}{\cos\theta_1 \sin\theta_3 + \sin\theta_1 \cos\theta_3}\dot{h}_Z
\end{aligned} \tag{13}$$

During singular conditions, nonsingular CMGs would operate normally per their decoupled steering logic. Take special care not to implement the equations listed below in a seemingly equivalent matrix form [Eq. (12)]. By calculating each CMG's proper command individually (rather than in a matrix), decoupled control steering allows nonsingular CMGs to be properly commanded during periods that other CMGs are singular. This can prevent loss of full attitude control and permits the momentum trajectory to pass the internal singular state.

X. Simulation of Singularity Reduction

Yaw maneuvers were simulated using typical coupled control and compared with the proposed decoupled control strategy. First, a +50 deg yaw maneuver is followed immediately by a −50 deg yaw maneuver, and then regulation at zero. The results of both methods are displayed in Fig. 16. Notice the coupled implementation of the Moore–Penrose pseudoinverse results in large unintended roll each time the momentum trajectory strikes the singular surface.

On the contrary, notice how decoupled control smoothly traverses the singularity surface with negligible roll or pitch errors. Since analysis and simulation both indicate the proposed decoupled control technique should work, experimental verification was performed on a free-floating spacecraft simulator (Figs. 17–19).

Notice in the simulation depicted in Fig. 16 that identical simulated experiments are compared, except one of the experiments used a coupled-matrix steering law (dotted line), while the second used uncoupled, individual steering equations to command each CMG (solid line). The thin line is hard to see when both experiments travel identical paths through the momentum space, but when the coupled-matrix steering law encounters a singularity, loss of attitude control results in large, undesired roll maneuvers. Underneath, it is easier to see the think line that represents the simulation using the uncoupled, individual steering equations, which cleanly passes through the singularity without loss of attitude control.

XI. Experimental Verification: Singularity Reduction via Decoupled Steering Technique

Experiments were performed with decoupled control to maximum momentum capability about the yaw axis. First note that Fig. 17 displays the ability of decoupled control steering to penetrate the singular surface associated with the coupled $[A]$ matrix of the CMG

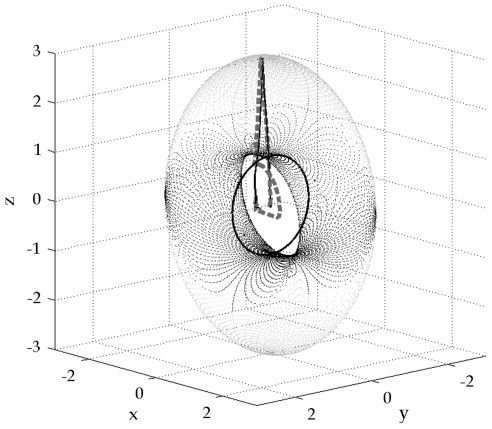

Fig. 16 Simulation: comparison of typical coupled control (dotted line) with decoupled control (solid line). Notice roll (x) errors when the momentum trajectory passes through the singularity resulting from loss of attitude control.

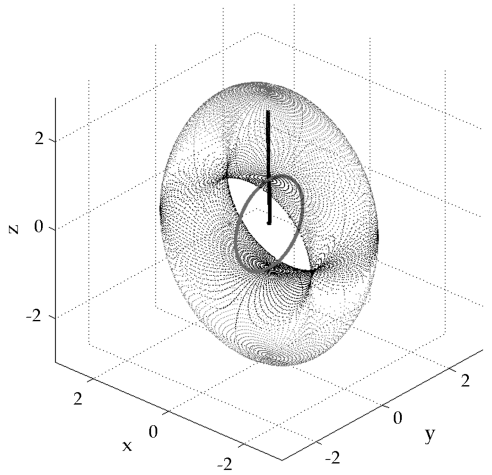

Fig. 17 Experimentation: demonstrated ability to pass cleanly through the singular surface at 1H using proposed decoupled control.

gimbal angles and skew angle. This attribute is exploited with an aggressive yaw maneuver (Fig. 18). The commanded yaw maneuver angle was increased 700% from ± 5 deg in 4 s to ± 35 deg in 10 s. This demands significantly more momentum change, specifically

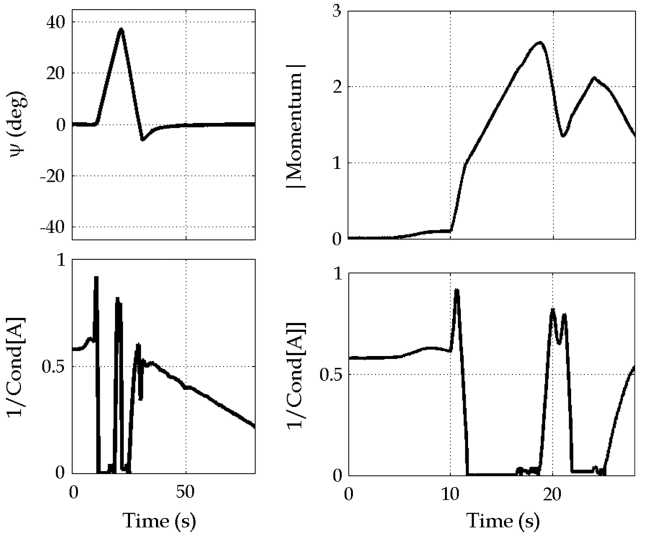

Fig. 18 Experiment: +35 deg yaw in 10 s, and −35 deg yaw in 10 s with decoupled steering.

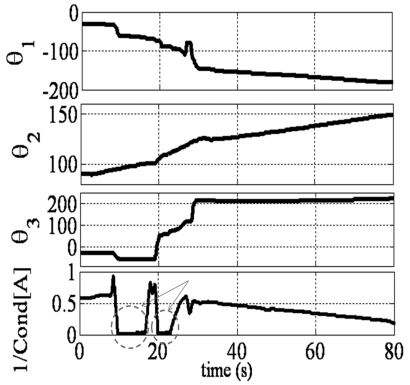

Fig. 19 Experiment: +35 deg yaw in 10 s, and −35 deg yaw in 10 s with decoupled steering. CMG gimbal angles and 1/cond[A].

about yaw. Figure 18 displays the required maneuver is achieved without incident. Notice that the coupled [A] matrix was singular twice during this maneuver.

Typical coupled control steering would have resulted in loss of spacecraft attitude control. Instead, with decoupled steering, you will notice a nice maneuver despite the singular [A] matrix. Attitude control is not lost at any time. Also notice the extremely high magnitude of momentum achieved without loss of attitude control associated with the passage of singularities.

XII. Conclusions

These experiments validate the much desired goal of CMG attitude control: extremely high torque without loss of attitude control associated with mathematical singularity. The optimized geometry is shown to increase singularity-free torque capability significantly. The maximized singularity-free momentum may be rotated to a preferred predominant maneuver direction by using mixed skew angles. Using a proposed decoupled control strategy, further singularity reduction is achieved that is shown to allow momentum trajectories to cleanly pass through singular surfaces without loss of attitude control. These claims were introduced analytically, and promising simulations were provided. Finally, experimental verification was performed, demonstrating maximal yaw maneuvers that passed through singular surfaces that would render loss of attitude control using typical coupled control techniques.

Acknowledgments

Special thanks go to Mike Pandolfo, U.S. Air Force, for manuscript review and editing. The views expressed in this paper are those of the authors and do not reflect the official policy or position of the U.S. Air Force, the U.S. Department of Defense, or the U.S. Government.

References

[1] Liska, D. J., and Dean, J., "Control Moment Gyros," Second Annual Meeting, AIAA Paper 1965-405, July 1965.

[2] Elrod, B. D., and Anderson, G. M., "Equilibrium Properties of the Skylab CMG Rotation Law-Case 620," NASA CR-126140, 1972, p. 79.

[3] Kennel, H. F., "Steering Law for Parallel Mounted Double-Gimbaled Control Moment Gyros," NASA TM-X-64930, 1975, p. 34.

[4] Colburn, B. K., and White, L. R., "Computational Considerations for a Spacecraft Attitude Control System Employing Control Moment Gyro," *Journal of Spacecraft and Rockets*, Vol. 14, No. 1, 1977, pp. 450–53.
doi:10.2514/3.57159

[5] Yoshikawa, T., "A Steering Law for Three Double Gimbal Control Moment Gyro System," NASA TM-X-64926, 1975.

[6] Kennel, H. F., "Steering Law for Parallel Mounted Double-Gimbaled Control Moment Gyros," NASA TM-X-82390, 1981, p. 22.

[7] Magulies, G., and Aubrun, J. N., "Geometric Theory of Single-Gimbal Control Moment Gyro System," *Journal of the Astronautical Sciences*, Vol. 26, No. 2, 1978, pp. 159–191.
[8] Tokar, E. N., "Problems of Gyroscopic Stabilizer Control," *Cosmic Research (Translation of Kosmicheskie Issledovaniya)*, 1978, pp. 141–147; also *Kosmicheskie Issledovaniya*, Vol. 16, No. 2, 1978, pp. 179–187.
[9] Kurokawa, H., Yajima, N., and Usui, S., "A CMG Attitude Control System for Balloon Use," *Proceedings of 14th International Symposium on Space Technology and Science (ISTS)*, AGNE Publ., Tokyo, 1984, pp. 1211–1216.
[10] Vadali, S. R., and Krishnan, S., "Suboptimal Command Generation for Control Moment Gyroscopes and Feedback Control Of Spacecraft," AIAA Guidance, Navigation, and Control Conference, AIAA Paper 1994-3615, Aug 1994, pp. 637–646.
[11] Seltzer, S. M., "Large Space Telescope Oscillation Induced by CMG Friction," *Journal of Spacecraft and Rockets*, Vol. 12, No. 2, 1975, pp. 96–105.
doi:10.2514/3.27815
[12] Paradiso, J., "A Search-Based Approach to Steering Single-Gimbaled CMGs," Charles Stark Draper Lab. TR CSDL-R-2261, Cambridge, MA, 1991, pp. 17, 26.
[13] Cornick, D. E., "Singularity Avoidance Control Laws for Single Gimbal Control Moment Gyros," AIAA Guidance and Control Conference, AIAA 1979-1968, 1979, pp. 20–33.
[14] Wie, B., *Space Vehicle Dynamics and Control*, 2nd ed., AIAA, Reston, VA, 1998, p. 439.
[15] Cornick, D. E., "Singularity Avoidance Control Laws for Single Gimbal Control Moment Gyros," AIAA Guidance and Control Conference, AIAA Paper 1979-1968, 1979.
[16] Hefner, R. D., and McKenzie, C. H., "A Technique for Maximizing the Torque Capability of Control Moment Gyro Systems," *Astrodynamics*, Vol. 54, Univelt, San Diego, CA, 1983, pp. 905–920.
[17] Kurokawa, H., Yajima, N., and Usui, S., "A New Steering Law of a Single Gimbal CMG System of Pyramid Configuration," *Proceedings of IFAC Automatic Control in Space*, Pergamon, New York, 1985, pp. 251–257.
[18] Paradiso, J., "Global Steering of Single Gimbaled Control Moment Gyroscopes Using a Directed Search," *Journal of Guidance, Control, and Dynamics*, Vol. 15, No. 5, 1992, pp. 1236–1244.
doi:10.2514/3.20974
[19] Paradiso, J., "A Search-Based Approach to Steering Single-Gimbaled CMGs," Charles Stark Draper Lab. TR CSDLR-2261, Cambridge, MA, 1991, p. 183.
[20] Bauer, S. R., "Difficulties Encountered in Steering Single Gimbal CMGs," *Space Guidance and Navigation Memo*, Charles Stark Draper Lab., 10E-87-09, Cambridge, MA, 1987.
[21] "A Comparison of CMG Steering Laws for High Energy Astronomy Observatories (HEAOS)," NASA TM X-64727, 1972, p. 127.
[22] Wie, B., "Singularity Robust Steering Logic for Redundant Single-Gimbal Control Moment Gyros," *Journal of Guidance, Control, and Dynamics*, Vol. 24, No. 5, Sept.–Oct. 2001, pp. 865–872.
doi:10.2514/2.4799
[23] Bedrossian, N. S., "Steering Law Design for Redundant Single Gimbal Control Moment Gyro Systems," NASA CR-172008, published by Charles Stark Draper Lab., Cambridge, MA, 1987.
[24] Bedrossian, N. S., Paradiso, J., Bergmann, E. V., and Rowell, D., "Steering Law Design for Redundant Single-Gimbal Control Moment Gyroscope," *Journal of Guidance, Control, and Dynamics*, Vol. 13, No. 6, 1990, pp. 1083–1089.
doi:10.2514/3.20582
[25] Magulies, G., and Aubrun, J. N., "Geometric Theory of Single-Gimbal Control Moment Gyro System," *Journal of the Astronautical Sciences*, Vol. 26, No. 2, 1978, pp. 159–191.
[26] Leve, F. A., and Fitz-Coy, N. G., "Hybrid Steering Logic for Single-Gimbal Control Moment Gyroscopes," *Journal of Guidance, Control, and Dynamics*, Vol. 33, No. 4, July–Aug. 2010, pp. 1202–1212.
doi:10.2514/1.46853
[27] Linden, S. P., "Precision CMG control for high-accuracy pointing," AIAA Guidance and Control Conference, AIAA Paper 1973-871, 1973, p. 7.
[28] Rybak, S. C., "Achieving Ultrahigh Accuracy with a Body Pointing CMG/RW Control System," AIAA Guidance and Control Conference, AIAA Paper 1973-871, 1973, p. 7.
[29] Vadali, S. R., Oh, H. S., and Walker, S. R., "Preferred Gimbal Angles for Single Gimbal Control Moment Gyros," *Journal of Guidance, Control, and Dynamics*, Vol. 13, No. 6, Nov.–Dec. 1990, pp. 1090–1095.
doi:10.2514/3.20583
[30] Seltzer, S. M., "CMG-Induced LST Dynamics," NASA TM-X-64833, 1974, p. 80.
[31] Seltzer, S. M., "Limit Cycle Analysis of Large Space Telescope with CMG Nonlinearity," NASA TM-X-64939, 1975, p. 20.
[32] Kurokawa, H., "Geometric Study of Single Gimbal Control Moment Gyroscopes," Mechanical Engineering Lab., Agency of Industrial Technology and Science, Ministry of International Trade and Industry TR 175, Japan7 June 1997.
[33] Bedrossian, N. S., Paradiso, J., Bergmann, E. V., and Rowell, D., "Steering Law Design for Redundant Single-Gimbal Control Moment Gyroscope," *Journal of Guidance, Control, and Dynamics*, Vol. 13, No. 6, 1990, pp. 1083–1089.
doi:10.2514/3.20582
[34] Magulies, G., and Aubrun, J. N., "Geometric Theory of Single-Gimbal Control Moment Gyro System," *Journal of the Astronautical Sciences*, Vol. 26, No. 2, 1978, pp. 159–191.
[35] Valadi, S. R., and Krishnan, S., "Suboptimal Command Generation for Control Moment Gyroscopes and Feedback Control of Spacecraft," Proceedings of AIAA Guidance, Navigation, and Control Conference, AIAA Paper 1994-3615, Aug. 1994, pp. 637–646.
[36] Paradiso, J., "Global Steering of Single Gimbaled Control Moment Gyroscopes Using a Directed Search," *Journal of Guidance, Control, and Dynamics*, Vol. 15, No. 5, 1992, pp. 1236–1244.
doi:10.2514/3.20974
[37] Takada, K., Kojima, H., and Matsuda, N., "Control Moment Gyro Singularity-Avoidance Steering Control Based on Singular-Surface Cost Function," *Journal of Guidance, Control, and Dynamics*, Vol. 33, No. 5, Sept.–Oct. 2010, pp. 1442–1450.
doi:10.2514/1.48381
[38] Sands, T., "Fine Pointing of Military Spacecraft," Ph.D. Dissertation, Mechanical and Astronautical Engineering Department, Naval Postgraduate School, Monterey, CA, 2007.
[39] Kojima, H., Matsuda, N., and Takada, K., "Adaptive Skewing Pyramid-Type CMGs for Fast Attitude Maneuver," *Transactions of the Japan Society for Aeronautical and Space Sciences*, Vol. 7, 2009, pp. 19–24.
doi:10.2322/tstj.7.19
[40] Kim, J. J., and Agrawal, B. N., "Acquisition, Tracking, and Pointing of Bifocal Relay Mirror Spacecraft," *Beam Control Conference Presentation*, Monterey, CA, Directed Energy Professional Soc., Albuquerque, NM, March 2006.
[41] Romano, M., and Agrawal, B. N., "Acquisition, Tracking, and Pointing Control of the Bifocal Relay Mirror Spacecraft," *Acta Astronautica*, Vol. 53, No. 4, 2003, pp. 509–519.
doi:10.1016/S0094-5765(03)80011-5